



Cite this: *Soft Matter*, 2017, 13, 2421

Received 16th January 2017,
Accepted 9th March 2017

DOI: 10.1039/c7sm00109f

rsc.li/soft-matter-journal

In situ observation of self-assembly of sugars and surfactants from nanometres to microns†

Samia Ouhajji,^a Jasper Landman,^{ab} Sylvain Prévost,^b Lingxiang Jiang,^c
Albert P. Philipse^a and Andrei V. Petukhov^{*ad}

The hierarchical self-assembly of sugar and surfactant molecules into hollow tubular microstructures was characterized *in situ* with high resolution small-angle X-ray scattering spanning more than three orders of magnitude of spatial scales. Scattering profiles reveal that aqueous host–guest inclusion complexes self-assemble into multiple equally spaced curved bilayers forming a collection of concentric hollow cylinders. Scattering data can be described by a simple theoretical model of the microtubes. The interlamellar distance was found to be surprisingly large. Moreover, we report that the multi-walled structure of the microtubes swells as the concentration or the temperature is varied.

The spontaneous formation of a complex ordered structure by self-assembly of disordered building blocks is a ubiquitous phenomenon in nature.¹ For instance, soap molecules self-organize into micelles, cell membranes are spontaneously formed by phospholipids and virus capsids, the nanosized containers protecting viral DNA, self-assemble inside infected cells.² A more complex example is provided by the tobacco mosaic virus. This rod-like virus consists of thousands of protein units that are joined together by a single RNA chain.³ This form of self-assembly, where several distinct spatial scales are involved, is known as hierarchical self-assembly. Highly ordered structures on the molecular, nanometre and micrometre scales can be formed by hierarchical self-assembly and could exhibit unique properties that are not inherent to the individual building blocks.³ The mechanical strength and toughness of bone, for example, is related to its hierarchical structure.⁴

Other examples include bamboo and nacre,⁵ architected metamaterials,⁶ hollow spherical micelles from rod-like block co-polymers,⁷ supramolecular polyhedra from DNA⁸ and responsive gels formed by peptides.⁹ In most cases, hierarchical self-assembly takes place in heterogeneous systems, where multiple components are needed to ensure self-assembly at different structural levels.

Another interesting example is provided by cyclodextrins and surfactants that exhibit hierarchical self-assembly in amphiphilic systems spanning several orders of magnitude of spatial scales.^{10–13} Cyclodextrins (CDs) are donut-like oligosaccharides with a hydrophilic outer surface and a hydrophobic cavity. CDs and surfactants can form aqueous host–guest inclusion complexes due to protection of the hydrophobic tail of the surfactants inside the hydrophobic cavity of CD. For example, two β -cyclodextrin (β -CD) molecules and one sodium dodecyl sulfate (SDS) molecule can spontaneously form host–guest complexes in water resulting in a SDS@2 β -CD inclusion complex with a completely hydrophilic exterior. Depending on the concentration of the complexes in aqueous solutions, various structures can be formed, including vesicles, microtubes and lamellae.^{10,13,14} The first two structures are formed due to bending of the lamellae in one or more directions presumably due to a trade-off between the energy required to curve the lamellae and the energy gained upon counterion condensation.¹⁵ It is unique that in this system the hierarchical self-assembly is homogeneous, *i.e.* occurring spontaneously by using a single building block, namely, the inclusion complex.

Here we demonstrate that synchrotron small-angle X-ray scattering (SAXS) is able to clearly resolve *in situ* all relevant scales of structural organization of simple sugar and surfactant molecules spanning length scales over three orders of magnitude. It was possible to follow the self-assembly starting with the formation of two-dimensional bilayers which are subsequently curved into three-dimensional multi-walled tubular structures ordered in a space-filling arrangement. Furthermore, the melting and swelling in the system due to variations in temperature and concentration, respectively, were studied.

^a Van 't Hoff Laboratory for Physical and Colloid Chemistry, Debye Institute for Nanomaterials Science, Utrecht University, Padualaan 8, 3584 CH Utrecht, The Netherlands. E-mail: S.Ouhajji@uu.nl, A.V.Petukhov@uu.nl

^b European Synchrotron Radiation Facility, 71 Avenue des Martyrs, 38000, Grenoble, France

^c Department of Materials Science and Engineering, Jinan University, Guangzhou 510632, China

^d Laboratory of Physical Chemistry, Eindhoven University of Technology, 5600 MB Eindhoven, The Netherlands

† Electronic supplementary information (ESI) available. See DOI: 10.1039/c7sm00109f

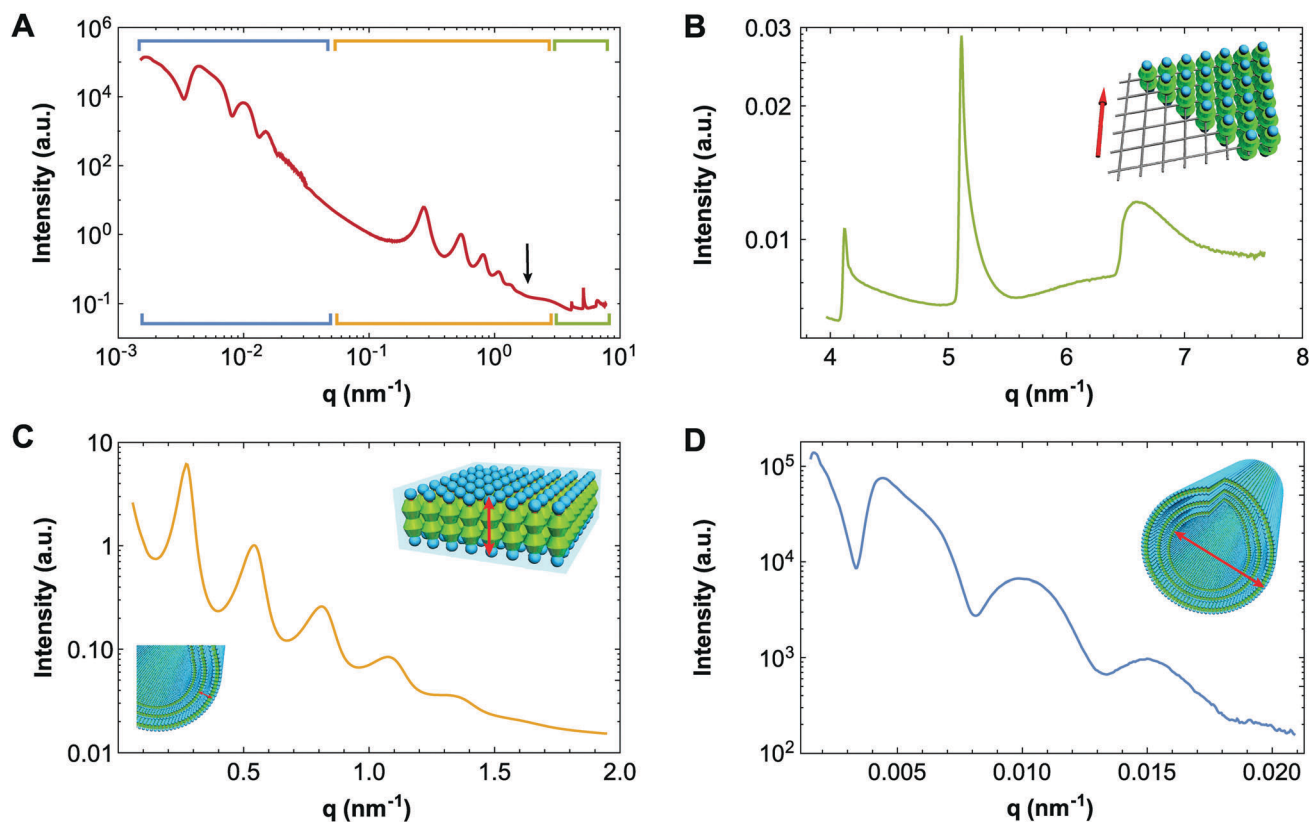


Fig. 1 SAXS measurements of 10 wt% SDS@2 β -CD complexes in water. (A) Radial intensity profile I as a function of wavevector q showing the complete set of data, measured using three sample-to-detector distances. The black arrow pinpoints the form factor minimum of the bilayers. (B) The saw-tooth shaped peak characteristic of 2D structures at high q . The inset shows the in-plane rhombic unit cell. (C) Inter- and intra-bilayer structure of the walls of the microtubes with a lamellar spacing of 23 nm. Insets show models of the bilayer and the multiwalled structure of the microtubes. The red arrows illustrate the bilayer thickness and interlamella distance. (D) At low q , the average diameter of the microtubes can be observed as indicated with the red arrow in the inset.

Fig. 1A gives an overview of the radial intensity profile, $I(q)$, of aqueous solutions of 10 wt% SDS@2 β -CD complexes measured at room temperature at a fixed position in the bulk. SAXS measurements were performed at beamline ID02 at the ESRF¹⁶ (see the ESI† for experimental details). Various regions are shown in more detail in Fig. 1B–D.

The SDS@2 β -CD complexes form 2D assemblies as revealed by the characteristic saw-tooth shaped peak in Fig. 1B; *i.e.* a peak with a rapidly rising edge at low angles followed by a continuous decrease toward larger scattering angles.^{17,18} At smaller angles, see Fig. 1C, a form factor minimum appears. The position of this minimum corresponds to a thickness of 3.5 nm, which is comparable to twice the length of an SDS molecule. This suggests that the walls of the 2D assemblies are composed of bilayers. Strong equidistant peaks are observed at intermediate angles and are characteristic of 1D periodicity (see Fig. 1C). These structure factor peaks are typically found in lamellar structures¹⁹ implying that our 2D assemblies consist of multiple equally spaced bilayers. Remarkably, the bilayers are a distance of 23 nm apart as can be deduced from the distance between adjacent peaks. As there is no (extra) added salt in the system, the large distances between the evenly spaced bilayers is thought to be due to counterion condensation.²⁰ Preliminary experiments with additional

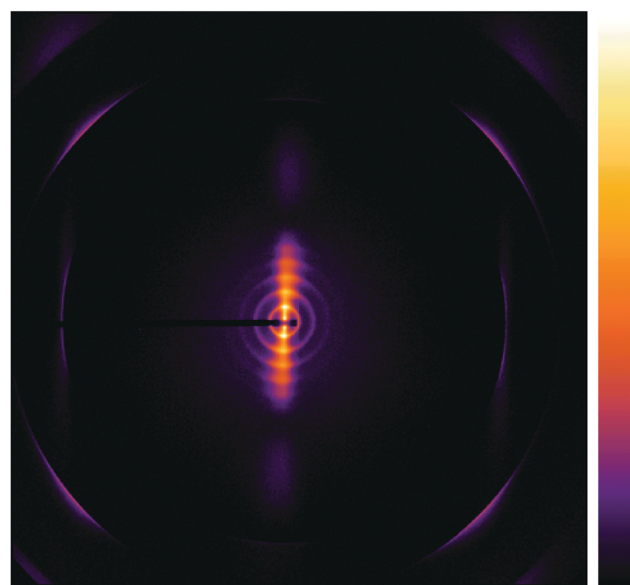


Fig. 2 2D SAXS pattern measured from a single domain near the capillary wall.

added salt have shown that the inter-bilayer distance decreases as the ionic strength increases, further strengthening our hypothesis.

Fig. 2 shows a 2D SAXS pattern recorded near the capillary wall. The tubular structures here are aligned parallel to each other due to anchoring at the wall of the capillary, making it possible to collect data from a single domain yielding an oriented scattering pattern. The positioning of the capillary results in horizontally aligned microtubes and bilayers that are rolled around the horizontal axis. The in-plane periodicity along the axis of the microtubes remains unaffected while the remaining diffraction peaks show broadening only in the vertical direction supporting the conclusion that the tubes are indeed rolled around the horizontal axis. The in-plane unit cell consistent with the 2D SAXS pattern can be indexed by a rhombus with $a = b = 1.52$ nm and $\gamma = 104^\circ$. A schematic representation of the unit cell is given in the inset of Fig. 1B. The average size of the tubes can be determined from the form factor minima observed at small angles as shown in Fig. 1D. The distance between these minima corresponds to 2π divided by $1.3 \mu\text{m}$, the latter manifesting in the presence of large objects on the order of a micrometre.

To further confirm that the microtubes consist of a multi-walled bilayer structure, the experimental scattering curve of the microtubes was fitted to the scattering of a hollow cylinder consisting of a number of evenly spaced concentric cylinders with wall thickness t_w and inter-bilayer periodicity s . The microtubes consist of n concentric cylinders with radius $R_j = R_0 + js$, with $0 \leq j \leq (n - 1)$ and R_0 denoting the radius of the innermost cylinder. The orientationally averaged X-ray scattering intensity is then proportional to²¹

$$I(q) \propto \frac{1}{q} \left(\sum_{j=0}^{n-1} \left(P_{R_j+t_w/2} - P_{R_j-t_w/2} \right) \right)^2, \quad (1)$$

where P_R is the orientationally averaged scattering amplitude of a full cylinder with radius R , given by

$$P_R(q) \propto \frac{R J_1(qR)}{q}. \quad (2)$$

Here, J_1 is the first order cylindrical Bessel function and q is the wave vector. Eqn (1) was used to fit the scattering data with the experimental parameters $t_w = 3.5$ nm and $s = 23$ nm. A reasonably accurate fit of the experiments was obtained using $n = 7$ concentric cylinders, $R_0 = 540$ nm and introducing polydispersity up to 10%. The experimental and theoretical scattering curves are shown in Fig. 3. For small wavevectors q , the fit revealed that the distance between these minima is equal to 2π divided by the average diameter of the microtubes defined as $2R_0 + (n - 1)s$, which is thus equal to $1.3 \mu\text{m}$.

The experimental and theoretical data deviate in two aspects. At the largest angles, the saw-tooth shaped peak is absent in the fit. This difference arises as a consequence of using homogeneous cylinders and not explicitly modelling the complexes composing the bilayers. In addition, a small but distinguishable peak can be seen at $q \cong 0.0044 \text{ nm}^{-1}$ in the experimental data only. Generally, the total scattering intensity is a combination of the form factor $P(q)$ and the structure factor $S(q)$ according to $I(q) \propto P(q) \times S(q)$. For dilute samples, the

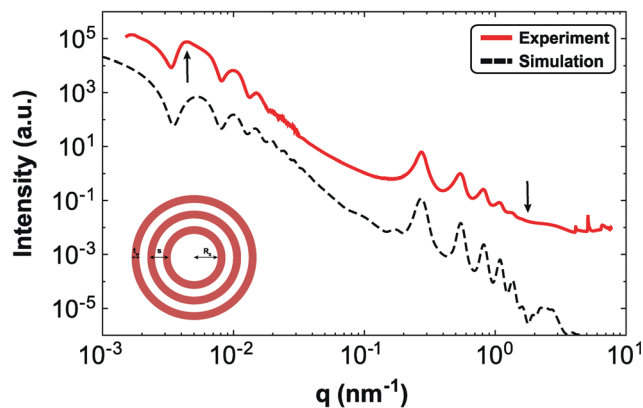


Fig. 3 Experimental and calculated scattering curves of 10 wt% microtubes. The fit does not show the saw-tooth shaped peak as this peak is a result of the apparent change in the distance between the complexes in the bilayer which is not taken into account in the model. For this fit, $t_w = 3.5$ nm, $s = 23$ nm, $n = 7$ and $R_0 = 540$ nm were used. The black arrows indicate the structure factor correlation peak and form factor minimum. The calculated curve has been offset vertically for the sake of clarity. Geometrical parameters in the model are introduced in the inset.

structure factor equals unity as structure correlations do not affect the scattering and eqn (1) holds. In all other cases, additional structure factor peaks will appear in the scattering intensity curve. Here, the structure factor correlation peak at small angles corresponds to a centre-to-centre distance between the microtubes of approximately $1.6 \mu\text{m}$. With a diameter of $1.4 \mu\text{m}$, the spacing between the microtubes is negligible and a space-filling arrangement is formed.

Finally, the response of the system to variations in concentration and temperature was probed. Aqueous solutions of SDS@2 β -CD complexes spontaneously self-assemble into hollow microtubes as long as the total concentration of β -CD and SDS is in the region between 6 and 25 wt%.¹⁴ To investigate the effect of concentration on the microtubes, scattering curves were recorded from well-aligned microtubes in suspension at varying concentrations. Fig. 4A shows that upon dilution of the system, *i.e.* as the SDS@2 β -CD complex concentration decreases from 20 to 10 wt%, swelling of the multiwall structure of the microtubes is observed. The periodicity between the bilayers making up the walls of the microtubes increases from 15 *via* 18 to 23 nm for 20, 15 and 10 wt% respectively as can be concluded from the shift of the equidistant structure factor peaks to larger angles. In addition, the overall diameter of the microtubes changes, as was confirmed by confocal microscopy images (see the ESI†). The microtubes grow by incorporating more SDS and cyclodextrin molecules into the walls which in turn become more compact to accommodate for the additional complexes upon increasing concentration. It must be noted that while the overall diameter of the microtubes grows, the pore diameter of the hollow tubes shrinks. Furthermore, the form factor minimum corresponding with the bilayer thickness, becomes more pronounced at higher concentrations of host-guest inclusion complexes.

As the formation of complex structures from SDS@2 β -CD complexes is thermo-reversible, it is thus possible to switch

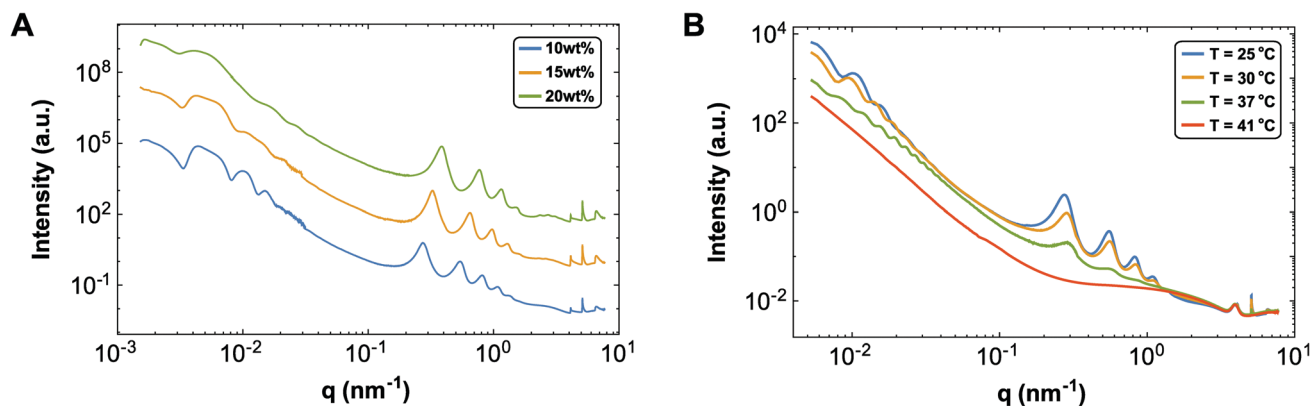


Fig. 4 The response of the thermo-reversible microtubes to variations in (A) concentration and (B) temperature. (A) Upon dilution of the microtubes, swelling of the multiwall structure is observed. The structure factor peaks at intermediate angles shift to larger wavevectors resulting in a larger inter-bilayer periodicity. The curves have been offset for the sake of clarity. (B) Above 40 °C, the characteristic features in the scattering curve disappear as the microtubes melt and fall apart. The broad peak around $q = 4 \text{ nm}^{-1}$ originates from scattering of the polyimide film (Kapton) on the window of the heating stage used during the temperature measurements.

between assembly and disassembly of the microtubes by simply changing the temperature. Above a temperature of 40 °C, the microtubes tend to melt as is confirmed by the featureless scattering seen in Fig. 4B. Below this threshold temperature, multiple oscillations can be observed. Initially, it was thought that these oscillations were due to formation of vesicles considering that Zhou and co-workers had previously shown that a reversible transition between vesicles and microtubes can be triggered by temperature.²² In their work, however, vesicles are dominant only above a temperature of 43 °C. Between 40 °C and 43 °C, a phase transition from microtubes to vesicles takes place and a mixture of both entities is obtained. Finally, at temperatures lower than the threshold temperature of 40 °C, vesicles are not formed at all.

On the other hand, the oscillations that are apparent in Fig. 4B are only present below this threshold temperature and disappear above 40 °C. Furthermore, the reported size of vesicles is much smaller than the characteristic size obtained from the scattering. Whereas bidisperse mixtures of vesicles with sizes of 700 and 200 nm were reported,¹⁰ here the oscillations are due to structures of approximately 1.7 μm . We hypothesize that these oscillations are due to radial enlargement of the microtubes upon heating, leading to monodisperse tubular structures with a well-defined radius.

In conclusion, we have studied in detail the hierarchical and thermo-reversible self-assembly of mixtures of sugar and surfactant molecules into microtubes using synchrotron SAXS. The self-assembly of this complex system could be characterized *in situ*, covering a total of more than three orders of magnitude of spatial scales, with one characterization technique. The microtubes consist of multiple equally spaced curved bilayers forming a set of concentric hollow cylinders in a space-filling arrangement. Moreover, we find that the bilayers composing the walls of the tubes are equally spaced but that the inter-bilayer distance is much larger than expected as a consequence of the highly charged system. Upon dilution of the microtubes, swelling of the multi-walled structure of the microtubes occurs.

Furthermore, the response of the system to variations in temperature was probed. The experimental data can be modelled with a simple concentric cylinder model. It is extraordinary that one technique, synchrotron SAXS, is capable of elucidating *in situ* the structure of a system while bridging so many orders of spatial scales. In the forthcoming studies, the application of SAXS to the co-assembly of colloids and SDS@2 β -CD microtubes will be investigated.²³

Acknowledgements

This work was supported by the Nederlandse Organisatie voor Wetenschappelijk Onderzoek (NWO) and the European Synchrotron Radiation Facility (ESRF). F. Chang and I. Rehor are thanked for their help with the SAXS measurements.

References

- 1 G. M. Whitesides and B. Grzybowski, *Science*, 2002, **295**, 2418–2421.
- 2 W. H. Roos, R. Bruinsma and G. J. L. Wuite, *Nat. Phys.*, 2010, **6**, 733–743.
- 3 J. A. A. W. Elemans, A. E. Rowan and R. J. M. Nolte, *J. Mater. Chem.*, 2003, **13**, 2661–2670.
- 4 Y. Liu, D. Luo and T. Wang, *Small*, 2016, **12**, 4611–4632.
- 5 U. G. K. Wegst, H. Bai, E. Saiz, A. P. Tomsia and R. O. Ritchie, *Nat. Mater.*, 2015, **14**, 23–36.
- 6 L. R. Meza, A. J. Zelhofer, N. Clarke, A. J. Mateos, D. M. Kochmann and J. R. Greer, *Proc. Natl. Acad. Sci. U. S. A.*, 2015, **112**, 11502–11507.
- 7 S. A. Jenekhe and X. L. Chen, *Science*, 1999, **283**, 372–375.
- 8 Y. He, T. Ye, M. Su, C. Zhang, A. E. Ribbe, W. Jiang and C. D. Mao, *Nature*, 2008, **452**, 198–202.
- 9 A. Aggeli, M. Bell, N. Boden, J. N. Keen, P. F. Knowles, T. C. B. McLeish, M. Pitkeathly and S. E. Radford, *Nature*, 1997, **386**, 259–262.

- 10 L. Jiang, Y. Peng, Y. Yan and J. Huang, *Soft Matter*, 2011, **7**, 1726–1731.
- 11 Y. Yan, L. Jiang and J. Huang, *Phys. Chem. Chem. Phys.*, 2011, **13**, 9074–9082.
- 12 L. Jiang, M. Deng, Y. Wang, D. Liang, Y. Yan and J. Huang, *J. Phys. Chem. B*, 2009, **113**, 7498–7504.
- 13 L. Jiang, Y. Yan and J. Huang, *Adv. Colloid Interface Sci.*, 2011, **169**, 13–25.
- 14 L. Jiang, Y. Peng, Y. Yan, M. Deng, Y. Wang and J. Huang, *Soft Matter*, 2010, **6**, 1731–1736.
- 15 F. Gobeaux, N. Fay, C. Tarabout, F. Meneau, C. Mériadec, C. Delvaux, J. Cintrat, C. Valéry, F. Artzner and M. Paternostre, *Langmuir*, 2013, **29**, 2739–2745.
- 16 P. Van Vaerenbergh, J. Leonardon, M. Sztucki, P. Boesecke, J. Gorini, L. Claustre, F. Sever, J. Morse and T. Narayanan, Proceedings of the 12th International Conference on Synchrotron Radiation Instrumentation (SRI2015), 2016, vol. 1741, p. 030034.
- 17 B. E. Warren, *Phys. Rev.*, 1941, **59**, 693–698.
- 18 J. K. Kjems, L. Passell and H. Taub, *Phys. Rev. B: Condens. Matter Mater. Phys.*, 1976, **13**, 1446–1462.
- 19 P. M. Chaikin and T. C. Lubensky, *Principles of Condensed Matter Physics*, Cambridge University Press, 2000.
- 20 G. S. Manning, *J. Phys. Chem. B*, 2007, **111**, 8554–8559.
- 21 E. Paineau, M. M. Krapf, M. Amara, N. V. Matskova, I. Dozov, S. Rouziere, A. Thill, P. Launois and P. Davidson, *Nat. Commun.*, 2016, **7**, 1–8.
- 22 C. Zhou, X. Cheng, Y. Yan, J. Wang and J. Huang, *Langmuir*, 2014, **30**, 3381–3386.
- 23 L. Jiang, J. W. J. de Folter, J. Huang, A. P. Philipse, W. K. Kegel and A. V. Petukhov, *Angew. Chem., Int. Ed.*, 2013, **52**, 3364–3368.